The EMBO Journal (2011) 30, 4084–4097 | © 2011 European Molecular Biology Organization | Some Rights Reserved 0261-4189/11
www.embojournal.org

THE EMBO JOURNAL

EMBO open

Splicing factor hnRNPH drives an oncogenic splicing switch in gliomas

Clare V LeFave[1,2], Massimo Squatrito[3,4], Sandra Vorlova[1], Gina L Rocco[1,2], Cameron W Brennan[3,5], Eric C Holland[3,4,5], Ying-Xian Pan[6] and Luca Cartegni[1,3,7,*]

[1]Department of Molecular Pharmacology and Chemistry, Memorial Sloan-Kettering Cancer Center, New York, NY, USA, [2]Weill Graduate School of Medical Sciences, Pharmacology Program, New York, NY, USA, [3]Brain Tumor Center, MSKCC, New York, NY, USA, [4]Department of Cancer Biology and Genetics, MSKCC, New York, NY, USA, [5]Department of Neurosurgery, MSKCC, New York, NY, USA, [6]Department of Neurology, MSKCC, New York, NY, USA and [7]Experimental Therapeutics Center, MSKCC, New York, NY, USA

In tumours, aberrant splicing generates variants that contribute to multiple aspects of tumour establishment, progression and maintenance. We show that in glioblastoma multiforme (GBM) specimens, death-domain adaptor protein Insuloma-Glucagonoma protein 20 (IG20) is consistently aberrantly spliced to generate an antagonist, anti-apoptotic isoform (MAP-kinase activating death domain protein, MADD), which effectively redirects TNF-α/TRAIL-induced death signalling to promote survival and proliferation instead of triggering apoptosis. Splicing factor hnRNPH, which is upregulated in gliomas, controls this splicing event and similarly mediates switching to a ligand-independent, constitutively active Recepteur d'Origine Nantais (RON) tyrosine kinase receptor variant that promotes migration and invasion. The increased cell death and the reduced invasiveness caused by hnRNPH ablation can be rescued by the targeted downregulation of IG20/MADD exon 16- or RON exon 11-containing variants, respectively, using isoform-specific knockdown or splicing redirection approaches. Thus, hnRNPH activity appears to be involved in the pathogenesis and progression of malignant gliomas as the centre of a splicing oncogenic switch, which might reflect reactivation of stem cell patterns and mediates multiple key aspects of aggressive tumour behaviour, including evasion from apoptosis and invasiveness.

The EMBO Journal (2011) **30,** 4084–4097. doi:10.1038/emboj.2011.259; Published online 13 September 2011
Subject Categories: RNA; molecular biology of disease
Keywords: antisense; cancer; FSD-NMD; hnRNPH; MADD; RON; splicing

Introduction

In mammalian genes, exons must be properly spliced together to generate mature mRNAs (Cartegni *et al*, 2002). Failure to effectively and accurately utilize splice sites can generate unstable and/or aberrant mRNAs encoding for defective or deleterious protein isoforms (Faustino and Cooper, 2003). Furthermore, splice sites can be differentially selected depending on developmental state, tissue and cell type, or in response to a wide array of physiological and pathological signals. Alternative splicing (AS) affects >75% of mammalian genes and is responsible for much of the proteome complexity (Pan *et al*, 2008). AS regulation ultimately depends on the intrinsic strength of the splice sites, on the presence of *cis*-regulatory elements (intronic and exonic enhancers and silencers), and on the combinatorial control by a discrete number of *trans*-activating factors, typically belonging to the serine/arginine-rich splicing factor (SR proteins) or the heterogeneous nuclear ribonucleoprotein (hnRNP) families (Martinez-Contreras *et al*, 2007; Long and Caceres, 2009).

A growing body of evidence suggests that dysregulated splicing patterns are also associated with tumourigenesis, with the appearance of hundreds of cancer-related isoforms. Multiple AS transcripts have been identified as progression markers, indicating both generalized splicing abnormalities or tumour- and stage-specific events (Venables *et al*, 2009).

Malignant transformation is dependent on the acquisition of specific capabilities, from uncontrolled growth, to escape from apoptosis, to metastatic invasion (Hanahan and Weinberg, 2000), typically obtained through mutations or genomic rearrangements. The same oncogenic effects can result from various epigenetic mechanisms, including the modification of AS patterns. In tumours, aberrant splicing usually arises from variations in the relative amounts/activity of regulatory splicing factors. Although a definitive causal relationship remains to be established for most cases, it is clear that the expression of specific splice variants of many cancer-related genes can directly contribute to the oncogenic phenotype and has a determinative role in many aspects of tumourigenesis and in the development of resistance to treatments (Ghigna *et al*, 2008).

Glioblastoma multiforme (GBM) is the most common type of primary brain cancer and is associated with a dismal prognosis, primarily due to its infiltrating properties and the emergence of resistance (Kanu *et al*, 2009). Treatment options have remained limited in part because of the still incomplete understanding of the basic biology of GBM. Given the complexity of splicing regulation in the brain, aberrant splicing in gliomas may be a significant but yet under-explored contributor to the heterogeneous pathological characteristics of GBM. Indeed, glioma-specific AS patterns (Cheung *et al*, 2008) have been reported, as well as additional aberrant splicing events that can contribute to all aspects of gliomagenesis, affecting angiogenesis (Huang *et al*, 2005), oncogenic suppression (Chunduru *et al*, 2002), escape from apoptosis (Yamada *et al*, 2003), proliferation (Camacho-Vanegas *et al*, 2007; Yu *et al*, 2007), metabolism (Clower *et al*, 2010; David *et al*, 2010) and migration/invasion (Yu *et al*, 2007; Cheung *et al*, 2009; Lo *et al*, 2009).

*Corresponding author. Department of Molecular Pharmacology and Chemistry, Memorial Sloan-Kettering Cancer Center, 1275 York Avenue, New York, NY, USA. Tel.: +1 646 888 2168; Fax: +1 646 422 0271; E-mail: cartegnl@mskcc.org

Received: 24 March 2011; accepted: 5 July 2011; published online: 13 September 2011

To better understand the role of AS deregulation in GBM, we looked at previously described splicing events that are altered in a variety of cancers and can generate variants with experimentally verified oncogenic properties. Here, we report that, in a large majority of human GBM samples and corresponding mouse models, exon 16 of the death-domain Insuloma-Glucagonoma protein 20 (IG20) transcript is differentially spliced to express the survival isoforms MAPK-activating death-domain-containing protein (MADD; Al-Zoubi *et al*, 2001).

IG20/MADD, an adaptor protein involved in TNF-α and TRAIL signalling (Mulherkar *et al*, 2007; Kurada *et al*, 2009), triggers apoptosis through caspase 8 activation (Al-Zoubi *et al*, 2001; Mulherkar *et al*, 2007). Alternative 5′ splice site usage in exon 13 combined with the inclusion/skipping of exon 16 generates four main splicing isoforms (Figure 1A), including MADD/DENN variants. While IG20 triggers apoptosis through caspase 8 activation, MADD variants are necessary and sufficient for cell survival *in vitro* and *in vivo* and their knockdown enhances TRAIL-induced apoptosis in cancer cells (Al-Zoubi *et al*, 2001; Lim *et al*, 2004; Mulherkar *et al*, 2006, 2007). MADD variants have been described to be aberrantly expressed in tumours (Efimova *et al*, 2004; Prabhakar *et al*, 2008; Kurada *et al*, 2009) and may thus constitute an important component of tumour escape mechanisms.

Splicing factors are often overexpressed in tumours and can directly behave as potent proto-oncogenes. SRSF1 (previously called SF2/ASF; Manley and Krainer, 2010) is upregulated in various human cancers and its overexpression is sufficient to transform rodent fibroblasts and cause high-grade sarcomas in nude mice (Karni *et al*, 2007). SRSF1 also directly modulates the expression of tumourigenic Recepteur d'Origine Nantais (RON) isoforms (Ghigna *et al*, 2005).

RON is the tyrosine kinase receptor for the macrophage stimulating protein (MSP), and is highly homologous to mesenchymal–epithelial transition receptor, whose activation in GBM is associated with shorter survival and poor prognosis (Kong *et al*, 2009). RON is a heterodimeric transmembrane receptor involved in cell proliferation, survival and the promotion of the epithelial–mesenchymal transition (EMT) and invasion (Lu *et al*, 2007). Exon 11 exclusion generates an isoform, RONΔ11 (RON165) that lacks part of the extracellular domain, resulting in a constitutive active isoform that promotes cell motility and mediates EMT (Ghigna *et al*, 2005).

In the present study, we describe that two oncogenic exonic silencing events (IG20 exon 16 and RON exon 11) occur in GBM samples and both can be controlled by the AS factor hnRNPH, which is overexpressed in gliomas. Control of these two splicing silencing events by hnRNPH can occur through an identical exonic splicing silencer (ESS) located at the 5′ end of the skipped exons, suggesting the same mechanism of action.

Our data suggest a novel role for hnRNPH as a splicing regulator in GBM biology, which can contribute to multiple pathological aspects of the GBM phenotype.

Results

AS of IG20/MADD exon 16 is altered in human and mouse gliomas

To study IG20/MADD AS in gliomas (McLendon *et al*, 2008; Lo *et al*, 2009), total RNAs from 20 GBM and 5 non-tumour brain samples were analysed by semi-quantitative reverse transcriptase PCR (RT–PCR). A representative result set for IG20/MADD exon 16 is shown in Figure 1B and a quantification of multiple experiments in Figure 1C, along with control PCRs. In non-tumour brain, we observed consistent levels of above 40% exon 16 inclusion (42.12 ± 1.442 s.e.m., $N = 5$), whereas inclusion of exon 16 in our 20 GBM samples dropped to a mean value of ~15% (15.08 ± 3.640 s.e.m., $N = 20$, pval = 5.11E-07; Figure 1C). This sharp decrease in exon 16 inclusion level was observed in 95% of the patient samples (19/20). On the contrary (Figure 1C; Supplementary Figure S1), no changes were observed when the AS pattern of IG20/MADD exon 13 was analysed (39.98 ± 0.9 versus 41.40 ± 2.1), suggesting that the two events are independently regulated and that switching to the tumourigenic MADD variant is specifically modulated in gliomas. As a positive control, we analysed FGFR1 exon-α splicing, a well-characterized AS event occurring in gliomas (Yamaguchi *et al*, 1994), which was similarly included less in GBM than in non-tumour brain (41.20 ± 4.620 versus 78.20 ± 1.428, pval = 1.27E-07; Figure 1C; Supplementary Figure S1).

Extension of the analysis of IG20/MADD AS to a panel of normal tissues and cell lines (Figure 1D) shows that exon 16 inclusion varies broadly in various tissues, from mostly skipped (e.g., thyroid) to mostly included (skeletal muscle), suggesting that this is a highly regulated and tissue-specific event. Furthermore, transformed cell lines show a more marked exon 16 skipping when compared with non-transformed ones (Figure 1D, right panel).

To investigate IG20/MADD exon 16 splicing in glioma mouse models, we took advantage of the RCAS/tva system, in which the RCAS avian leukosis virus mediates somatic gene transfer into cells expressing the viral receptor (tva) (Dai and Holland, 2001). Localized delivery of RCAS retroviruses expressing the PDGF-B gene into the brain of newborn transgenic mice producing the tva receptor under control of the early glial lineage nestin promoter (*N-Tva*) gives rise to glial tumours (Dai and Holland, 2001; Shih *et al*, 2004). When PDGF-B is expressed in *N-Tva* mice with *Ink-4a-Arf* null background (*N-Tva Ink-4a-Arf*$^{-/-}$) or with conditional PTEN knockout background (*N-Tva* LP, together with RCAS-Cre), tumour initiation and progression is promoted, yielding higher grade gliomas (Hu and Holland, 2005). These GBM-like features are enhanced by the combination of both backgrounds (*N-Tva Ink-4a-Arf*$^{-/-}$ LPTEN; Hambardzumyan *et al*, 2009).

Similarly to what observed in human GBM samples, we determined that RNAs derived from the PDGF-driven high-grade tumours showed a consistent switch towards IG20/MADD exon 16 skipping when compared with RNAs from control brains of the same genotype, where PDGF-B was not expressed (Figure 1E, compare lanes 1–3 with lanes 4–8 or 9–13 and quantification below).

IG20/MADD exon 16 contains multiple regulatory elements

The mechanism(s) controlling IG20/MADD AS are currently unknown. To identify regulatory *cis*-elements that modulate exon 16 splicing and the corresponding *trans*-acting factors, we generated a minigene construct containing the 3061-nt genomic region spanning IG20/MADD exons 15–17, with the entire intervening introns (Figure 2A). Transient expression

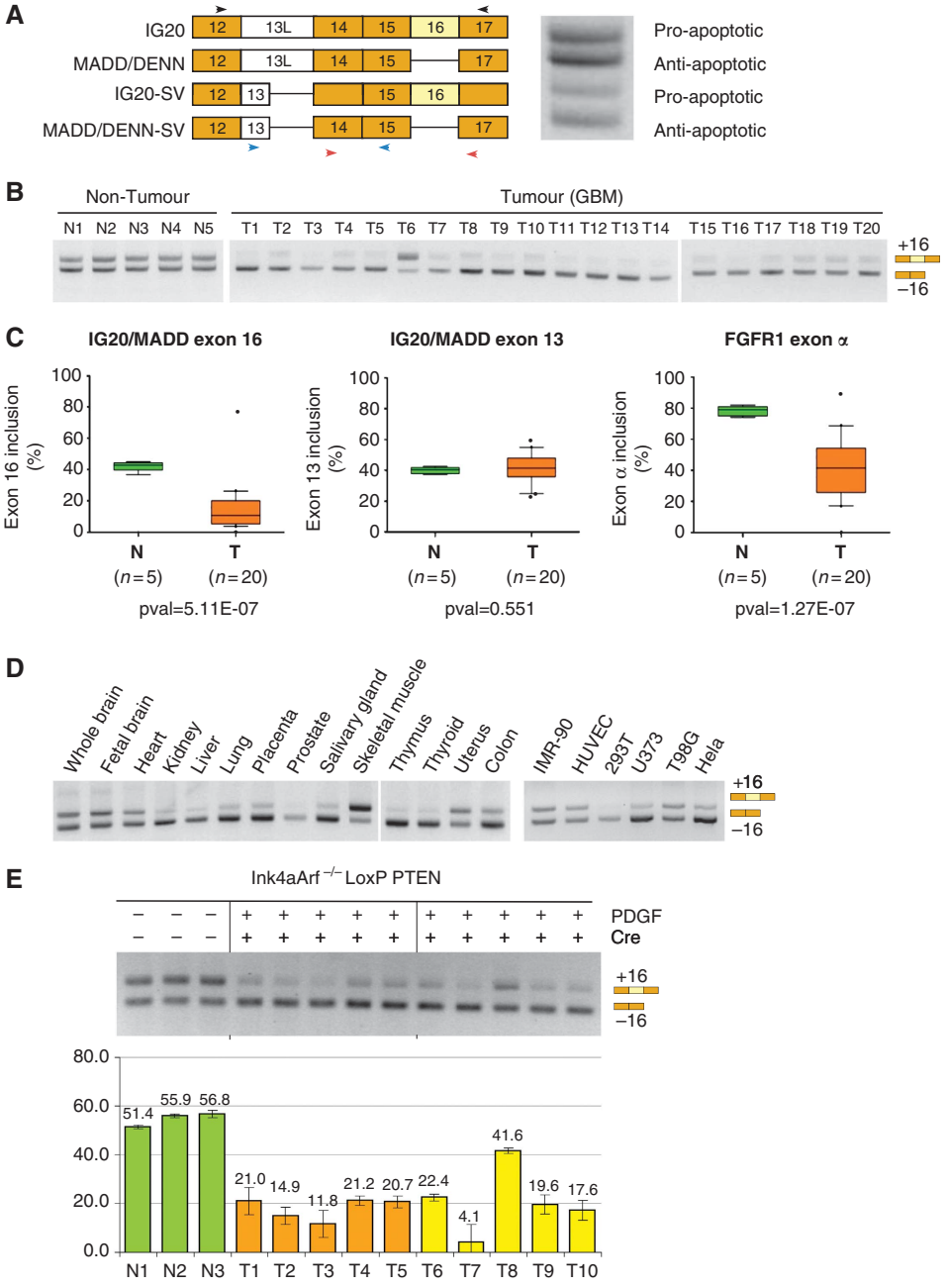

Figure 1 IG20/MADD exon 16 alternative splicing is altered in gliomas. (**A**) Schematic of the exon structure of four IG20/MADD isoforms generated by AS of exon 13 (alternative 5′ss) and exon 16 (exclusion). RT–PCR using primers flanking exons 13 and 16 (black arrows) shows the splicing pattern of the four isoforms in HeLa cells. Arrows indicate approximate position of primer pairs. (**B**) Total RNAs from human normal brain ($n=5$) and GBM samples ($n=20$) were analysed by RT–PCR for IG20/MADD exon 16 splicing pattern using primer sets on exons 14 and 17 (red arrows in **A**). Representative gels are shown. (**C**) Quantification of data from (**B**) for AS of IG20/MADD exon 16 (left), IG20/MADD exon 13L (middle) and positive control FGFR1 α-exon (right). Three PCRs were quantified and averaged for each sample. The 90/10/median box and whiskers plot was then calculated for the normal ($n=5$) and tumour ($n=20$) sets using Prism software. The 90/10/median shows the variation of exon inclusion of the calculated normal and tumour sets. Indicated *P*-values were determined by two-tailed Student's *t*-test. (**D**) IG20/MADD exon 16 splicing pattern (as in **B**) from the indicated human tissues and cell lines. (**E**) Three independent mouse brain samples of the *N-tva* Ink-4a-Arf$^{-/-}$ LoxP PTEN background were examined for AS of the murine IG20/MADD exon 16 pattern along five independent samples each from brain tumour developed in the same genetic background following RCAS-PDGF and RCAS-PDGF + RCAS-CRE delivery. In short, all samples are Ink-4a-Arf null and tumours are driven by PDGF-B overexpression alone or concomitant to PTEN downregulation. RT–PCR experiments using murine IG20 primers in exons 14 and 17 were repeated in triplicate, and a representative gel is shown with the average quantification of the exon 16 inclusion is below. The drops from inclusion levels in the normal brain (green columns) to the levels in the two tumour groups (orange and yellow columns) are highly statistically significant (pvals = 1.57E-16 and 4.27E-08, respectively).

of this synthetic pre-mRNA yielded a splicing pattern comparable to the endogenous transcripts (~10% inclusion, Figure 2B, lanes 1 and 2), indicating that most relevant regulatory elements are maintained in the minigene. Strengthening of the weak pyrimidine tract of exon 16 by a double mutation (Figure 2A, Py^), resulted in full exon 16

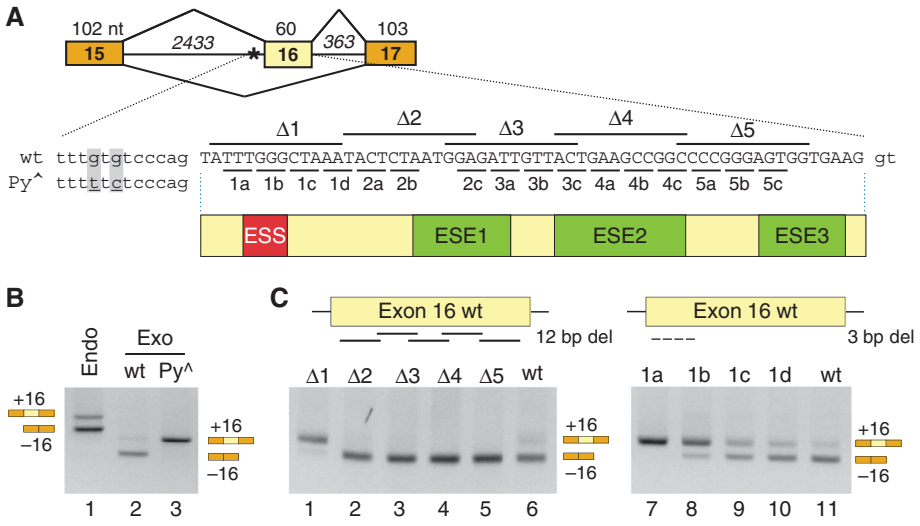

Figure 2 Identification of regulatory exonic splicing elements in IG20/MADD exon 16. (**A**) Diagram of AS of IG20/MADD minigene (top) with the sizes (nt) indicated. Wild-type (wt) and pyrimidine enhanced (Py^) partial minigene sequences are shown (lowercase and uppercase letters represent introns and exons, respectively). Lines above and below the exon 16 sequence indicate exact position of the 12-nt (Δ1–Δ5, above) and 3-nt (1a–5c, below) deletions generated. Red and green boxes represent the approximate mappings of the identified putative ESS and of the three putative ESEs. (**B**) Splicing pattern of endogenous IG20/MADD exon 16 (endo) and transfected wt and Py^ minigenes (exo) in HeLa cells. For the endogenous products, primers on exons 14 and 17 are used, for the minigene product, plasmid-specific primers are used. (**C**) RT–PCR analysis of exon 16 deletion mutants within the wt-minigene context, transfected into HeLa cells. The positions of the deletions on exon 16 are indicated.

inclusion (Figure 2B, lane3), suggesting that its incorporation depends on efficient recognition of the splice sites.

Then, we used these minigenes as the basis for a systematic mutational analysis of exon 16. A first set of partially overlapping deletions (Δ1–Δ5) was introduced from position +3 to +55 (Figure 2A). Deletion Δ1 lead to a dramatic switch to full exon 16 inclusion (Figure 2C, lane 1) identifying this region as a putative ESS. Smaller deletions encompassing Δ1 narrow the putative silencer to the TTTGGG sequence from position 3 to 9 of the exon (Figure 2C, lanes 7 and 8). Deletions Δ2–Δ5 are associated with a reduction in exon 16 inclusion (Figure 2C, lanes 2–5), suggesting the presence of exonic splicing enhancers (ESEs). To better study these elements, we inserted the same deletions in the context of the Py^ mutant, where the basal level is full inclusion, and confirmed that ablation of any of the Δ2–Δ5 regions inhibits exon 16 inclusion (Supplementary Figure S2A). Smaller deletions analysed in the same context revealed the presence of three distinct ESEs in exon 16 (Supplementary Figure S2B). A bioinformatics analysis of the sequence using enhancer-predicting algorithms identified three clusters of putative enhancer elements that colocalize with the regions identified by deletion analysis (Supplementary Figure S2C). However, overexpression of putative regulating splicing factors SRSF1, SRSF5 and SRSF6 leads to no changes in exon 16 splicing (Supplementary Figure S2D). A comparable mutational analysis using larger deletions (100/500 nt) spanning most of the upstream intron did not yield any candidate intronic regulatory element (Supplementary Figure S3).

IG20/MADD exon 16 silencer is controlled by hnRNPH

To characterize the silencer revealed by the TTT and GGG deletion, we analysed by transient transfection a complete panel of mutants where every position was independently changed to all three other nucleotides (Figure 3A and B).

When any of the Gs from the G-triplet (G_6–G_8 in the exon) were mutated, exon 16 skipping dropped from ~90% to <25%. On the contrary, mutation of the second T of the element (T_4 in the exon) has no effect on the splicing pattern, whereas mutation of the first T (T_3 in the exon) leads to high levels of inclusion only if changed to G (Figure 3A and B, lane 1 panel G). Since the preceding nucleotide in the exon is an A, this mutant introduces an AG just three nucleotides downstream of the natural AG. Sequencing of the corresponding PCR product revealed in fact that this additional AG is efficiently used as an alternative 3′ splice site (Supplementary Figure S4). Mutation of the third T (T_5 in the exon) to A or C strongly inhibits exon 16 skipping, while on the contrary transversion to a G promotes even stronger exon skipping (Figure 3A and B, lane 3 panel G), indicating that the T is important in maintaining the silencing activity, but it can be substituted by a G. A pseudo-frequency matrix of the four nucleotides in the six different positions was derived from the exon 16 inclusion quantitation data and the WebLogo 3.0 algorithm (Crooks *et al*, 2004) was used to generate a consensus motif pictogram (Figure 2C).

The consensus sequence T/G GGG corresponds to the well-characterized binding motif of hnRNPH/F proteins (Chen *et al*, 1999; Caputi and Zahler, 2001). HnRNPH is an RNA-binding protein involved in multiple aspects of RNA metabolism. The splicing activity of hnRNPH is highly context dependent and can both inhibit or promote usage of specific splice sites from either intronic or exonic positions (Fogel and McNally, 2000; Mauger *et al*, 2008; Fisette *et al*, 2010). A radioactively labelled 24 nt RNA probe spanning the putative hnRNPH binding site, incubated with nuclear extract, formed a slow-migrating complex, identified by electrophoretic mobility shift assay (EMSA; Figure 3D, lane 2). This complex is competed away by excess amount of unlabelled RNA of the same sequence (lanes 4 and 5),

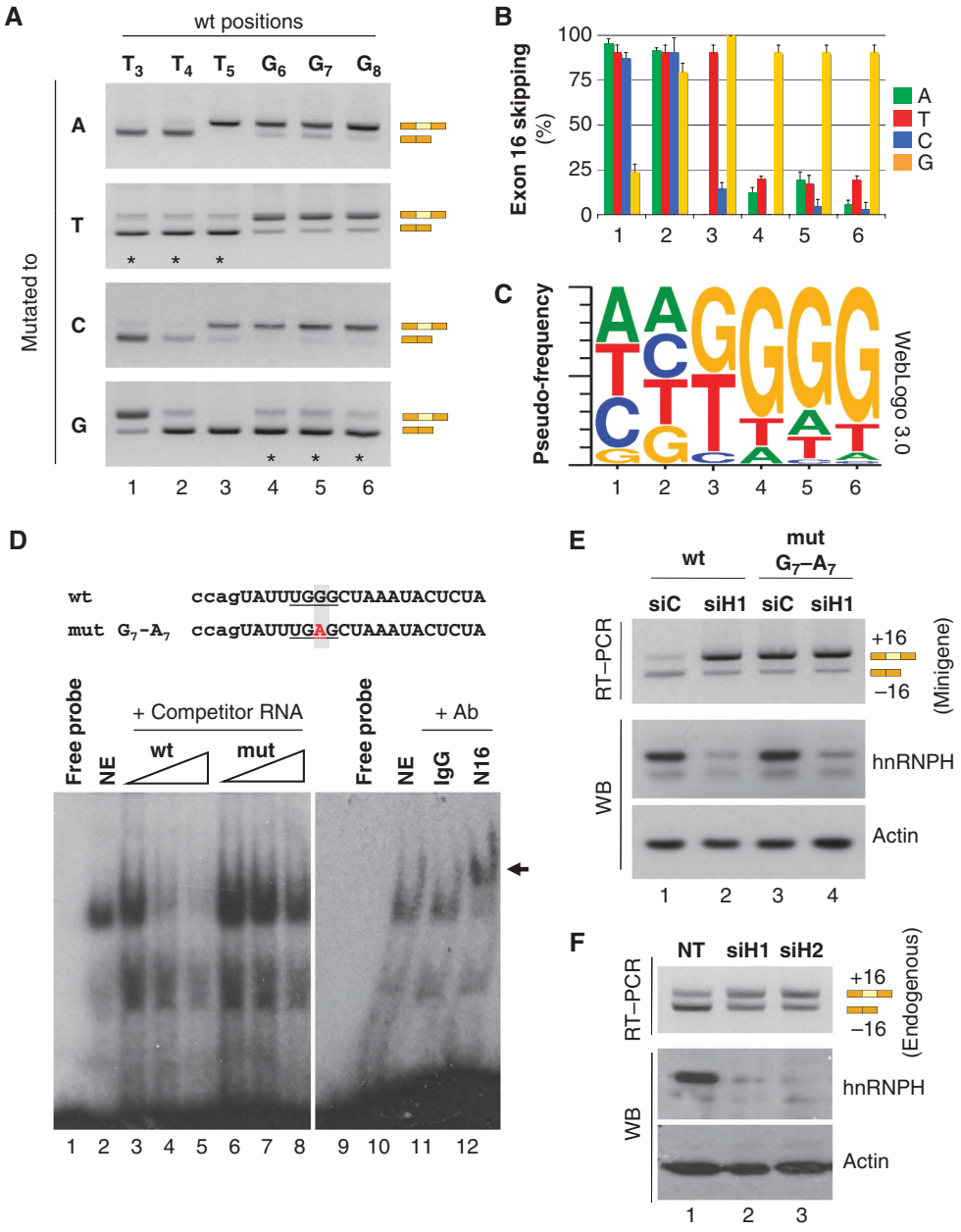

Figure 3 The ESS in IG20/MADD exon 16 is controlled by hnRNPH. (**A**) RT–PCR analysis of mutant minigenes harbouring single-point mutations generated within deletions 1a and b (Figure 2A and C) upon transient transfection in HeLa cells. Top indicates the wt nucleotide and the position within IG20/MADD exon 16. Left-down indicates the nucleotide each position is mutated to. *Indicates that the wild-type nucleotide was maintained. Representative gels of three independent transfections experiments are shown. (**B**) Quantification of point mutations made in (**A**) represented as percent of exon 16 skipping; data are average of three independent experiments, ± s.d. (**C**) Representation of a pseudo-frequency matrix obtained from data in (**B**), generated using WebLogo 3.0. (**D**) EMSA of radiolabelled wt-probe mock treated (lanes 1 and 9), or incubated with HeLa nuclear extract (lanes 2 and 10), with × 20, × 100 or × 400 excess of unlabelled wild-type (wt) or mutant (mut) probes (lanes 3–5 and 6–8, respectively), with a control IgG (lane 11) or with hnRNPH-specific antibody N-16 (lane 12). Supershifted band is indicated by arrow. RNA sequences for the wt and mut probes are shown on top with the putative hnRNPH binding site region underlined, and mutation in red. (**E**) Wt IG20/MADD minigene and G_7–A_7 mutant (Figure 2A, lane 5 panel 'A') co-transfected with control siRNAs (siC) or with siRNAs to HnRNPH (siH1). RT–PCR of exogenous IG20/MADD exon 16 splicing (top), western blots for total hnRNPH (middle) and actin (bottom). (**F**) HeLa cells were separately treated with two individual siRNAs to hnRNPH, twice 24 h apart and then RNAs were collected at 72 h for analysis. Top, RT–PCR analysis of endogenous MADD exon 16 splicing. Bottom, two panels are western blot analyses of hnRNPH and actin.

but not by equal amounts of a mutant RNA comprising the single G-to-A mutation within the UGGG motif (Figure 3D, lanes 7 and 8), previously shown to induce exon 16 inclusion (Figure 3A, lane 5). Inclusion of antibodies specific to hnRNPH, but not of control antibodies, induced a supershift in the migration profile, demonstrating that the complex formed around the UGGG motif includes hnRNPH (Figure 3D, lanes 11 and 12).

SiRNA-mediated knockdown of hnRNPH leads to a net increase in exon 16 inclusion from the wild-type minigene, but not from the G-to-A mutant (Figure 3E). Endogenous IG20/MADD splicing was also similarly affected when either

of two hnRNPH-targeted siRNAs was used (Figure 3F). Attempts to overexpress hnRNPH were not very successful, perhaps because of the presence of negative feedback mechanisms to regulate its levels (Ni *et al*, 2007). However, co-transfection of a plasmid encoding hnRNPH with the IG20 minigene was associated with a further decrease in exon 16 inclusion in the wt, but not in the mutant construct (Supplementary Figure S5) even if the levels of hnRNPH were not obviously elevated.

Based on these observations and on abundant data that show that hnRNPH can act directly through such motifs in regulating splicing, we conclude that hnRNPH limits exon 16 inclusion by binding to the UGGG-containing silencer at the 5′ end of exon 16.

HnRNPH protects from cell death via MADD activity

Since MADD promotes cell survival, whereas IG20 promotes apoptosis, the switch from MADD to IG20 driven by hnRNPH depletion should result in reduced cell viability. Indeed, compared with control siRNA treatments, knockdown of hnRNPH by siH1/2 (Figure 4A, lanes 2 and 5), led to a significant increase in cell death both in U373 glioma cells and in HeLa cells (U373: 2.2 ± 0.20-fold increase, pval = 0.00012; HeLa: 3.9 ± 0.97-fold increase, pval = 6.43E-05; Figure 4C) that remarkably parallels the improved exon 16 inclusion (quantified in Figure 4B).

HnRNPH controls a broad number of targets, many of which are still unknown. To test whether the increase in cell death is directly caused by the change in IG20/MADD splicing, rather than by other unrelated hnRNPH-dependent events, we combined knockdown of hnRNPH with isoform-specific knockdown of IG20, using an siRNA targeted to exon 16 (siE16). When siE16 was combined with the siRNAs targeting hnRNPH (siH1/2), downregulation of the IG20 isoform led back to IG20/MADD RNA ratios similar to those of control-related cells (Figure 4A and B, lanes 1 versus 3 and 4 versus 6), regardless of hnRNPH levels (top western). This switchback in the splicing profile is associated with robust rescue from hnRNPH-induced cell death in both cell types (Figure 4C, lanes 3 and 6), indicating that hnRNPH not only significantly promotes cell survival, but also that its action is specifically mediated by inhibiting inclusion of IG20 exon 16.

RON exon 11 splicing is also controlled by hnRNPH

When we examined other AS variants differentially expressed in tumours and suggested to have a role in various aspects of tumourigenesis, we found that RON exon 11 was also significantly more excluded in GBM samples than in non-tumour samples (Figure 5A and B, 44.07 ± 3.324 s.e.m. versus 60.03 ± 4.981, pval = 0.0258), although the change was not as homogeneous as in the case of IG20/MADD. We were unable to reliably detect the mRON transcripts by RT–PCR in mouse samples, but when we examined the splicing pattern of RON in human normal tissues and cell lines (Supplementary Figure S6) levels of exon 11 exclusion were overall lower in the tissues and more normal cell lines (IMR90 and HUVEC) but increased in other cell lines, in particular glioma cell lines U373 and T98G.

Alignment of the sequences of IG20/MADD exon 16 and RON exon 11 revealed a striking homology at their 5′ ends (Figure 5C): the first 10 nucleotides of IG20 exon 16

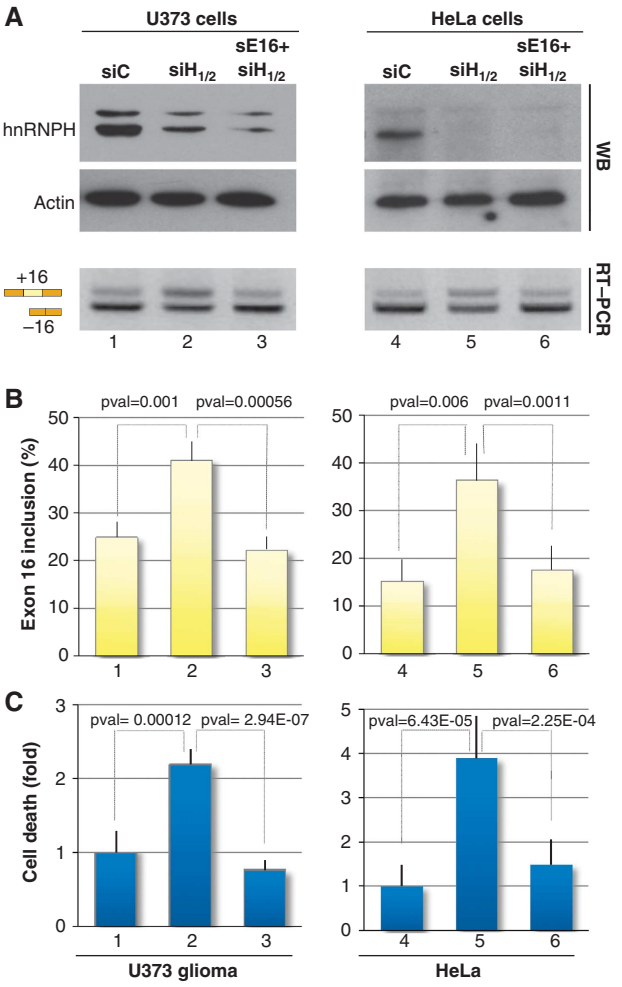

Figure 4 HnRNPH regulates IG20-dependent cell death through IG20/MADD splicing. (**A**) U373 glioma cells (left) and HeLa cells (right) were treated for 72 h with the indicated siRNAs (siH1/2 = siH1 + siH2). HnRNPH knockdown was assessed by western blot using actin as a loading control. The pattern of IG20/MADD exon 16 splicing was analysed by gel electrophoresis and a representative gel is shown on the bottom. (**B**) Exon 16 inclusion was quantified from multiple biological replicates (U373, $n = 6$; HeLa, $n = 7$) and is represented as average percent of exon 16 inclusion (± s.d.). (**C**) Cell death from the experiments in (**B**) was determined by trypan blue assay and is represented as fold change of control treatment (± s.d.). *P*-values were calculated by two-tailed Student's *t*-test.

(cag|TATTTGGGCT) are present in identical positions in RON exon 11 (cag|TATATTGGGCT), except for a single insertion at position 4. Both regions include the TGGG motif recognized by hnRNPH (underlined), in addition RON also contains a second TGGG motif just 2 nt downstream and two more in positions 32 and 50 of the exon. Indeed, hnRNPH knockdown was associated with a complete switch to endogenous exon 11 inclusion (Figure 5D).

To validate the role of the putative silencer, we cloned the RON genomic region from exon 10 to exon 12 (Figure 5E). The transfected minigene is less efficiently spliced than the endogenous counterpart, probably due to the very short introns, but like endogenous RON, the spliced product from the minigene shows preferential exon 11 skipping (Supplementary Figure S7A, lane 1). Mutation of either of the TGGG motifs to TGAG promoted exon inclusion, which

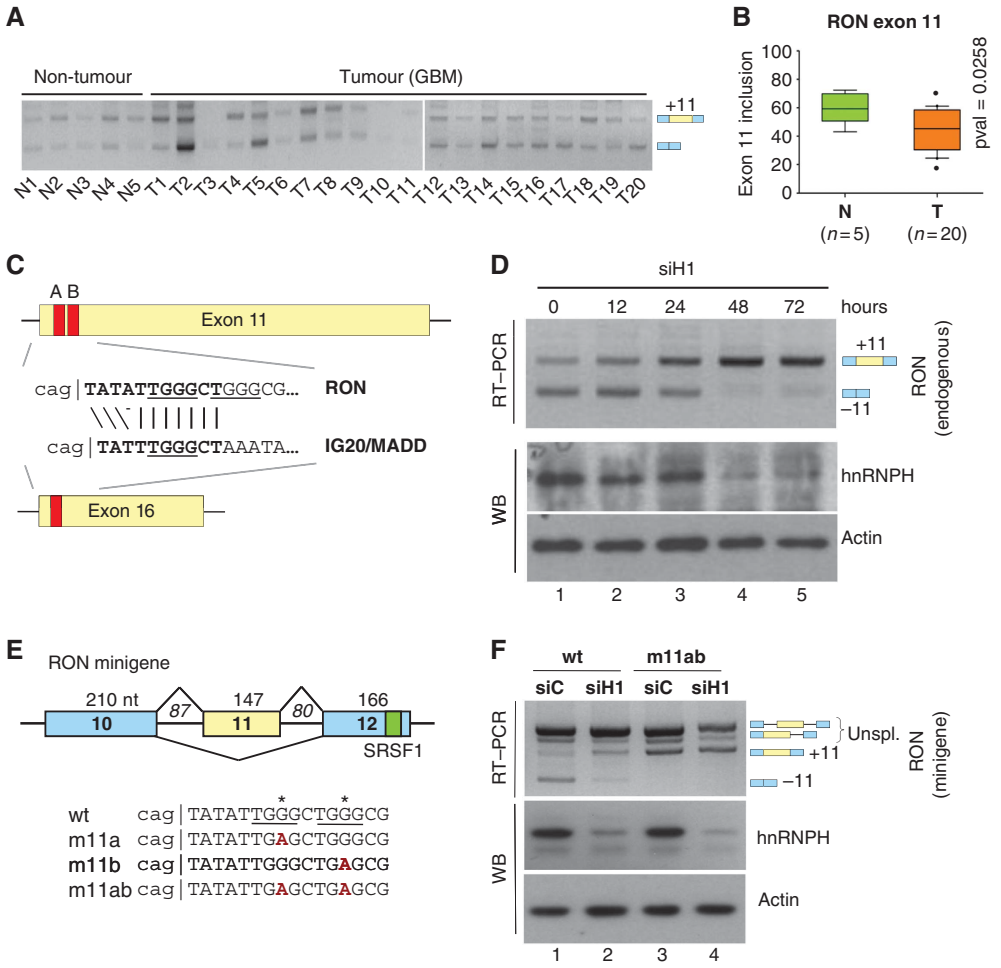

Figure 5 A similar ESS in RON exon 11 is also controlled by hnRNPH. (**A**) Total RNAs from normal brain ($n=5$) and GBM samples ($n=20$) were analysed by RT–PCR for AS of RON exon 11 using primer sets on exons 10 and 13. The difference in size is due to exon 11 skipping. Representative gels are shown. (**B**) Quantification of data from (**A**) for AS of RON exon 11, as in Figure 1C. (**C**) Alignment of the 5′ regions of RON exon 11 and IG20 exon 16 with the TGGG motifs underlined (indicated by red boxes). (**D**) RT–PCR analysis of endogenous RON exon 11 splicing pattern from samples treated with siRNAs to hnRNPH (siH1) for up to 72 h (top). Western blot analysis of hnRNPH expression levels (middle) from the same treatments, with actin as loading control (bottom). (**E**) Schematic of AS of RON exon 11 minigene with exon and intron sizes and the SRSF1 binding site indicated (top). *Indicates the position of the RON minigene A and B G-to-A mutations within the TGGG motif, where m11a is 5′ to m11b and m11ab is a combination of the two. (**F**) Wt RON minigene and m11ab double mutant (from) co-transfected with control siRNAs (siC) or with siRNAs to hnRNPH (siH1). RT–PCR of exogenous RON exon 11 splicing (top), western blots for total hnRNPH (middle) and actin (bottom).

was highest when both mutations were combined (Figure 5F, lane 3; Supplementary Figure S7A). SiRNA knockdown of hnRNPH also improves exon inclusion from the transfected wt RON minigene, but has no effect on the m11ab mutant (Figure 5F). Conversely, when hnRNPH was co-transfected with the wt minigene exon inclusion was reduced (Supplementary Figure S7B), whereas there was no promotion of exon skipping when the m11ab mutant was used (Supplementary Figure S7B).

Splicing factor SRSF1 was previously shown to regulate RON exon 11 by binding to a downstream regulatory element on exon 12 (Ghigna *et al*, 2005). Exon 12 also contains a silencing region that includes GGG triplets. When the core Gs were independently mutated in three of these elements, a moderate increase in exon 11 skipping was observed in 2/3 cases (Supplementary Figure S8A), suggesting a role in antagonizing the action of SRSF1 from exon 12, perhaps also through hnRNPH (Supplementary Figure S8B). However, the strong effect of hnRNPH on exon 11 splicing is not via SRSF1, as its levels are not affected by hnRNPH knockdown (Supplementary Figure S9).

Together, these data support a model where hnRNPH controls RON exon 11 splicing through the same mechanism used in the modulation of IG20/MADD exon 16, by binding to UGGG elements in the 5′ region of the alternative spliced exon.

HnRNPH knockdown by FSD-NMD

Binding of MSP to RON leads to its phosphorylation and activation, resulting in the upregulation of multiple signalling pathways and processes, like cellular proliferation and migration (Wagh *et al*, 2008). Expression of the Δ11 isoform activates RON independently of ligand binding (Ghigna *et al*, 2005). To test whether hnRNPH also controls the biological properties of RON, we designed a 'splicing switchback' experiment analogous to that described in Figure 4. In the case of RON, however, isoform-specific knockdown is not an optimal approach because, while MADD and IG20 have

antagonistic functions and downregulation of one isoform results in increase of the activities dependent on the second one, RON and RONΔ11 have different requirements (ligand binding) to exert the same downstream activity. Therefore, elimination of one isoform does not imply activation of the other one. One way to bypass this problem is to directly induce a splicing switch by a splicing redirection approach using modified antisense oligonucleotides such as phosphorodiamidate morpholino oligomers (morpholinos) (Kinali *et al*, 2009).

In principle, appropriately designed morpholinos should be able to induce skipping of any internal exon, including constitutive ones. If skipping an exon leads to a premature termination codon (PTC), the variant mRNA would be destabilized by non-sense mediated decay (NMD). To minimize non-specific effects due to the treatments, we applied this new forced splicing-dependent NMD (FSD-NMD) approach to hnRNPH knockdown as well as a standard splicing re-redirection approach to modulate RON exon 11 inclusion, rather than to combine siRNA and morpholino treatments.

Failure to include exon 4 in hnRNPH mRNA induces a frameshift that leads to a PTC in exon 5 (Figure 6A). Accordingly, when morpholinos directed at the 3′ (H4.3′) and 5′ splice sites (H4.5′) bordering exon 4 were delivered to HeLa cells, they induced significant downregulation of hnRNPH at both the RNA and protein level (Figure 6B). When the two compounds were used in combination, they resulted in an almost complete knockdown of hnRNPH expression (Figure 6B, lane 4), at least as good as that obtained by a standard siRNA approach (Supplementary Figure S9). Like siRNA-mediated knockdown, FSD-NMD downregulation of hnRNPH induces inclusion of RON exon 11 and IG20 exon 16, but not of IG20 exon 13 (Supplementary Figure S9), and does not affect expression of the closely related hnRNPF or of SRSF1.

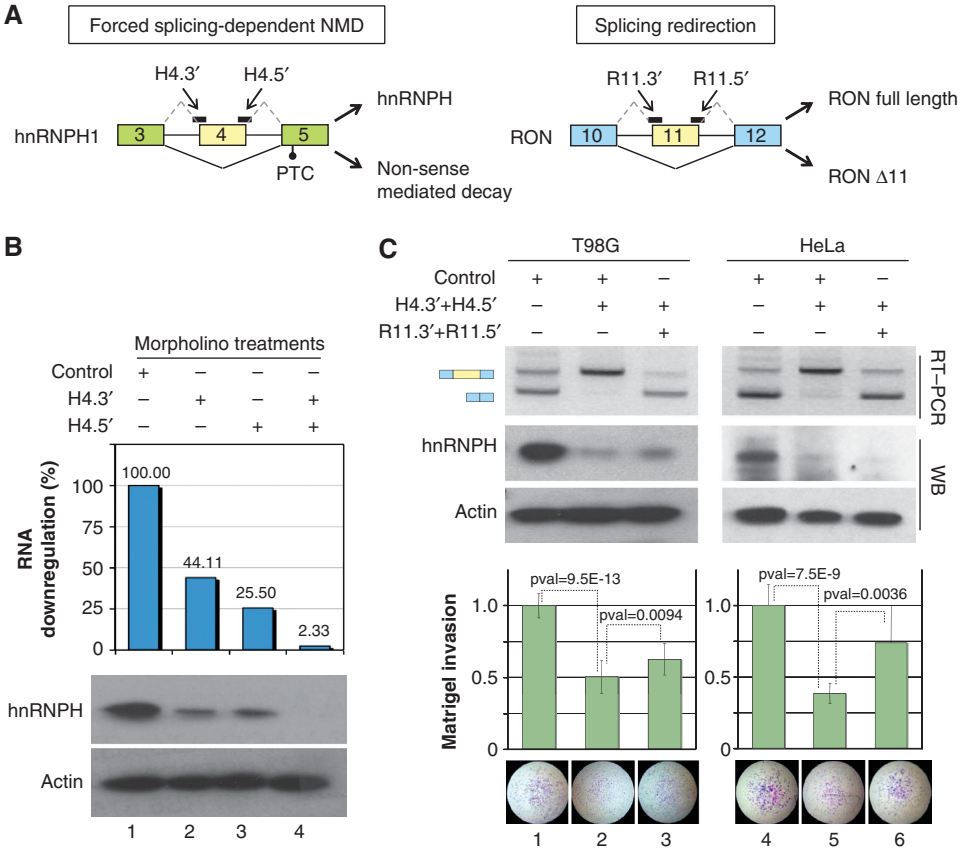

Figure 6 FSD-NMD knockdown of hnRNPH reduces invasiveness *via* RON exon 11 splicing. (**A**) Left: FSD-NMD knockdown of hnRNPH. Morpholinos targeted to hnRNPH exon 4 splice sites (H4.3′ and H4.5′) cause skipping of exon 4, leading to a frameshift and a PTC in exon 5, and ultimately causing RNA degradation by NMD. Right: splicing redirection. Morpholinos targeted to RON exon 11 splice sites (R11.3′ and R11.5′) induce in-frame skipping of exon 11, resulting in two protein products: ligand-dependent full-length RON and ligand-independent RONΔ11. (**B**) Knockdown of hnRNPH by FSD-NMD in HeLa cells after 72 h of treatment (control, H4.3′, H4.5′ and combined H4.3′ + H4.5′). The abundance of hnRNPH RNAs following FSD-NMD morpholino treatment was quantified by qPCR and represented as percent downregulation of control treatment (average of two independent experiments). Bottom panels: western blot analysis of hnRNPH protein levels, with actin as loading control. (**C**) T98G glioma cells and HeLa cells were treated with control morpholinos (lanes 1 and 4), with the H4 pair of hnRNPH knockdown morpholinos (lanes 2 and 5) and with the H4 pair combined with R11 pair of RON splicing redirection morpholinos (lanes 3 and 6). The effect of treatments on RON exon 11 splicing pattern (RT–PCR), and on hnRNPH or actin levels (western blots) was analysed. The same cells were also analysed for their invading capabilities using a matrigel invasion assay (bottom panel). Invading cells were stained with crystal violet and scored blind. Values were then normalized to the control for each experiment. Averages of normalized scores from 15 (5 experiments in triplicate) and 9 (3 experiments in triplicate, ± s.d.) matrigel inserts are represented for T98G and HeLa cells, respectively. *P*-values were determined by a two-tailed Student's *t*-test.

HnRNPH promotes invasion via RON activity

Next, we designed morpholinos (R11.3′ and R11.5′) to induce RON exon 11 skipping (Figure 6A). After treatment of glioblastoma T98G or HeLa cells with the H4 morpholino pair for 72 h, hnRNPH strong downregulation was associated with a near complete switch to RON exon 11 inclusion in both cell lines (Figure 6C, lanes 2 and 5). When downregulation of hnRNPH by the H4 pair was combined with the R11 morpholino pair, the level of exon 11 inclusion reverted to control, even in the absence of hnRNPH (Figure 6C, lanes 3 and 6). To assess invasiveness potential, treated cells were starved for 6 h and equal numbers of live cells (to control for cell death due to the hnRNPH knockdown) were seeded onto matrigel in a transwell/Boyden chamber. After 24 h, cells were scored blind for migration (Figure 6C). Knockdown of hnRNPH reduces the invading capability of T98G and HeLa cells to 50.5% (pval = 9.5E-13) and ~38.4% (pval = 7.5E-9) of control-treated cells, respectively (Figure 6C, lanes 2 and 5). Induction of RON exon 11 skipping partially but significantly rescues the ability of both cell types to migrate through matrigel to ~62.3 and 73.9, respectively (pvals = 0.0094 and 0.0036; Figure 6C, lanes 3 and 6), showing that hnRNPH levels contribute to the invading properties of glioblastoma and other cancer cells, at least in part through modulation of RON exon 11 splicing.

HnRNPH is overexpressed in gliomas

The data on IG20/MADD and RON show that at least two splicing events controlled by hnRNPH are aberrant in GBM. Quantitation of hnRNPH RNA levels in 20 GBM samples and 5 normal brains by Quantitative PCR (qPCR) revealed a significant increase in hnRNPH RNA levels in GBM (pval = 0.0096; Figure 7A), consistent with the observed switches in splicing. This result is reinforced by data extracted from the Oncomine database (http://www.oncomine.org), where 3/5 sets that compare expression in GBM with normal brain show highly significant increase in hnRNPH levels (pval < 1E-5; Shai *et al*, 2003; Bredel *et al*, 2005; Sun *et al*, 2006) while the other two show increase (Liang *et al*, 2005; Lee *et al*, 2006), but at lower significance (pvals = 0.068 and 0.034, respectively), possibly due to the limited number of normal samples (Figure 7B). Overexpression of hnRNPH in human GBM samples was also confirmed at the protein level by immunohistochemical analysis of graded human glioma specimens (Figure 7C; Supplementary Figure S10). HnRNPH expression correlates with morphologically determined tumour grades, with very low levels in normal brain, medium levels in low-grade and high levels in high-grade tumours.

Finally, we also examined hnRNPH expression in lysates from whole brain or from brain tumours derived from *N-Tva Ink-4a-Arf*$^{-/-}$ LPTEN mice injected with RCAS-PDGF alone or in combination with RCAS-Cre, where PDGF overexpression results in high-grade gliomas (as described above). The expression of hnRNPH is strongly induced in 5/5 lysates derived from the tumours obtained by overexpression of PDGF-B and loss of PTEN (Figure 7D, lanes 1–3 versus 4–8) and in 4/5 lysates from overexpression of PDGF-B alone (Figure 7D, lanes 1–3 versus 5–8), consistent with its proposed role in mediating IG20/MADD exon 16 exclusion (Figure 1E).

Altogether, we show that altered levels of hnRNPH are present in human GBM and GBM mouse models. This might explain some of the aberrant splicing events observed in these tumours and could contribute to significant pathological aspects of this disease, such as escape from apoptotic stimuli and increased mobility and invasiveness.

Discussion

The connection between deregulation of AS and tumour development is emerging as a novel and important aspect of cancer biology. The major question raised by the large amount of data that correlate aberrant splicing variants to tumour progression remains that of the causal relationship between splicing deregulation and disease. The data presented in this work directly support the notion of a causative role for at least two such splicing events as part of a common oncogenic splicing switch driven by RNA-binding protein hnRNPH: the induction of a pro-survival variant of death-domain adaptor protein IG20-MADD and of a motility-enhancing isoform of RON receptor tyrosine kinase.

HnRNPH oncogenic effects via IG20/MADD and RON splicing

We observed consistent aberrant MADD splicing in human GBM samples and mouse tumours. Rigorous mapping of splicing regulatory elements identified an ESS at the 5′ end of MADD exon 16, which mediates exon skipping *via* a core U/G GGG motif. The G-triplet is necessary but not sufficient to induce silencing and requires a preceding T or G. HnRNPH, which is upregulated in gliomas, can be part of a complex assembled on the UGGG motif to inhibit exon 16 inclusion, and similarly controls RON exon 11 splicing, also aberrant in gliomas.

HnRNPH influences the processing of a broad range of mRNAs in multiple ways, depending on context. In general, intron-bound hnRNPH activates splicing of upstream exons (Wang and Cambi, 2009) or stimulates intron excision by promoting homotypic and heterotypic interactions that loop out intronic regions (Martinez-Contreras *et al*, 2006; Fisette *et al*, 2010). In contrast, hnRNPH represses splicing when bound to exons (Chen *et al*, 1999; Mauger *et al*, 2008), as shown here with MADD and RON, by antagonizing activities from nearby enhancers, by directly interfering with spliceosome components or by nucleating a silenced region through high-affinity binding followed by RNA propagation, as proposed for hnRNP A1 (Okunola and Krainer, 2009).

The positioning and striking homology of the two ESSs suggest that the regulation of both IG20/MADD exon 16 and RON exon 11 splicing events are carried out by hnRNPH in a like manner. The more marked effect of hnRNPH depletion on RON, compared with IG20/MADD, could be due to the presence there of additional UGGG motifs, and the full switch to exon 11 inclusion also indicates that, in this context, related members of the hnRNPH protein family, such as hnRNPF, H2 and H3, cannot fully compensate for the loss of hnRNPH expression (hnRNPF levels are not affected by hnRNPH downregulation; Supplementary Figure S9). We were unable to specifically downregulate hnRNPF, but it remains possible that any the hnRNPH/F family member also binds the ESS and contribute to MADD (and RON) aberrant splicing in tumours. In fact, hnRNPF is strongly upregulated in 9/10 of the mouse tumours analysed (Supplementary Figure S11), suggesting that the regulation

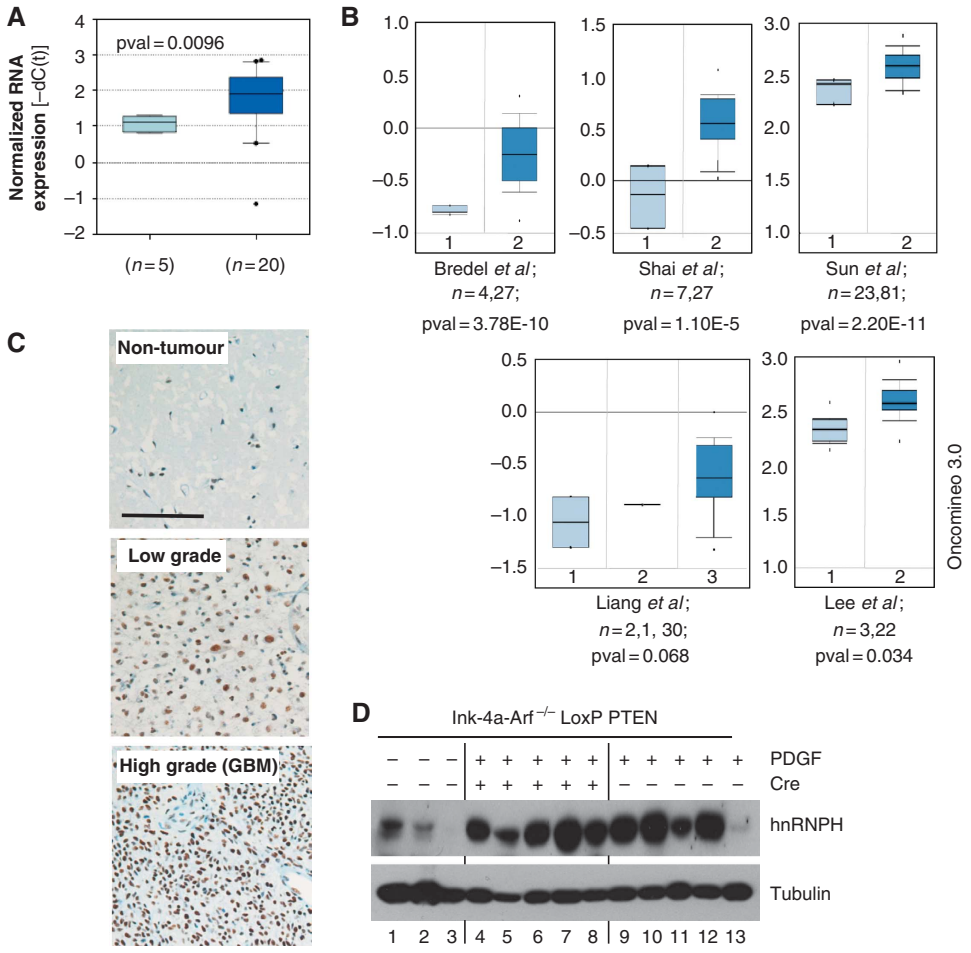

Figure 7 HnRNPH is overexpressed in gliomas. (**A**) qPCR analysis of hnRNPH expression in normal ($n = 5$) and GBM ($n = 20$) RNAs. Results were normalized to the housekeeping gene rps3 and are represented as −dCt. (**B**) HnRNPH expression from five microarray studies. Oncomine™ (Compendia Bioscience, Ann Arbor, MI) was used for analysis and visualization. Bredel *et al*: brain (1), GBM (2). Shai *et al*: white matter (1), GBM (2). Sun *et al*: brain (1), GBM (2). Liang *et al*: brain (1), cerebellum (2), GBM (3). Lee *et al*: neural stem cells (1), GBM (2). Expressed as normalized expression units. (**C**) Immunohistochemistry analysis of human normal brain, low-grade glioma and high-grade glioma (GBM) samples using anti-H antibodies. Scale bar indicates 100 μm. For a larger panel of samples analysed, see Supplementary Figure S10. (**D**) Western blot analysis of samples from Figure 1E, using anti-hnRNPH antibodies, with tubulin shown as loading control.

of hnRNPH and hnRNPF might be coordinated. Conversely, a reduction in exon 16 inclusion could also be achieved by inhibiting the unknown factor(s) that recognize the additional ESEs on exon 16 (Supplementary Figure S2C). All three ESEs share the core purine-rich motif GRAG (R = G, A) common to many SR-dependent enhancers, and might indicate that a single protein or complex recognizes all three sites (although SRSF1, SRSF5 and SRSF6 do not appear to be involved, at least *in vitro*; Supplementary Figure S2D). In all, 15/20 of the individual GBM samples show a good correlation between expression levels of hnRNPH and exclusion of Ig20/MADD exon 16, compared with non-tumour samples (Supplementary Figure S12). However, four tumours have high levels of exon 16 skipping but not of hnRNPH RNAs, indicating that aberrant IG20/MADD splicing can be controlled by multiple factors, especially in highly heterogeneous tumours like GBM.

To show that the role of hnRNPH and the changes in MADD and RON can be causative with respect to survival and invasiveness, we designed experiments to selectively manipulate the endogenous splicing events. Knockdown of hnRNPH using two independent methods (RNAi and FSD-NMD) induced increased inclusion of the cancer-skipped exons and was associated with decreases in cell viability and migration in glioma and other cancer cells. To move from a correlation to a causative role, we separately rescued each of them, using isoform-specific RNA interference and a splicing redirection strategy. The 'switchback' of the splicing pattern was followed by a reversal of the biological readout involved (cell death for MADD and invasion for RON), thus demonstrating the causal relationship. Obviously, this does not exclude that hnRNPH might also affect other targets important in GBM biology, in particular some involved in the modulation of cell motility, as suggested by the only partial rescue of migratory defects in hnRNPH-ablated T98G cells.

The IG20/MADD switch in gliomas could provide advantageous to cancer cells because of the role of IG20/MADD in TRAIL receptor signalling. TRAIL contributes to immune-surveillance and effectively induces apoptosis of cancer cells. Unfortunately, gliomas and other cancers acquire TRAIL resistance through a variety of molecular alterations

that include mutations in the receptor complex, expression of decoy receptors and overexpression of survival factors. The switch from IG20 to MADD not only prevents caspase 8 activation, but also simultaneously promotes the MAPK and NFκB pathways, effectively converting an environmental death signal into a growth/survival one. The antagonist functions of IG20/MADD splicing variants raise the possibility of re-sensitizing TRAIL-resistant cells to TRAIL treatment, either by inhibiting the activity of hnRNPH or other regulatory factors, or by directly interfering with the splicing event itself—as shown in this work—using an antisense-based splicing redirection approach, which is emerging as a powerful technology for manipulation of gene expression *in vitro* and *in vivo*, with great therapeutic potential (Hua *et al*, 2008; Kinali *et al*, 2009; Wu *et al*, 2009).

HnRNPH upregulation

Our data clearly show that the downregulation of hnRNPH is sufficient to modulate both MADD and RON splicing to reduce their more tumourigenic variants, suggesting for hnRNPH a direct role in enhancing tumour aggressiveness by inhibiting apoptosis and promoting invasion.

To elucidate the role played by hnRNPH and—more broadly—by AS deregulation in tumourigenesis, it is important to understand the underlying causes. Aberrant splicing in cancer is typically associated with changes in the abundance/activity of the regulatory splicing factors by multiple mechanisms (copy number, transcription and phosphorylation). This non-specifically generates a large pool of splicing variants with diverse functions, from where traits providing a growth or survival advantage can be selected for. Alternatively, some of these AS changes may correspond to improper activation of regulated AS in cancer cells, for example ones that reflect developmental gene expression regulatory mechanisms typical of stem cells, and therefore contribute to the 'stemness' of cancer cells in gliomas and other tumours.

Comparison of AS patterns between human embryonic stem cells and differentiated neural progenitors revealed significant changes and indicated that the loss of pluripotency affects RNA splicing factors themselves, including intron retention events in the hnRNPH and H3 genes and the switch from MADD to IG20 (Yeo *et al*, 2007; Salomonis *et al*, 2009). Indeed, differentiation of BE2 brain tumour cells by Retinoic Acid is associated with a reduction in hnRNPH expression and an increase in IG20 exon 20 inclusion (Supplementary Figure S13). This is the opposite switch that we observed in tumours, supporting the idea that some of the tumour-specific AS events may correspond to reactivation of early developmental patterns controlled by a network of splicing factors which could include hnRNPH and hnRNPI/PTB (polypyrimidine tract binding protein) another well-established regulator of splicing. A switch from PTB to nPTB in post-mitotic neurons regulates multiple splicing events (Boutz *et al*, 2007; Coutinho-Mansfield *et al*, 2007) and PTB is reactivated in gliomas (Cheung *et al*, 2006), where it contributes to proliferation and invasion (Jin and Cote, 2004; Cheung *et al*, 2009). Consistently, hnRNPH/F levels are temporally reduced in postnatal brain development (Wang *et al*, 2007; Wang and Cambi, 2009) but elevated in aggressive gliomas (this work), and are high in mouse undifferentiated mesenchymal cells but quickly downregulated upon smooth muscle differentiation (Liu *et al*, 2001).

Based on these observations and on the remarkable consistency of the AS switch to MADD in glioblastoma samples as well as its occurrence in the mouse models, we suggest that this event likely reflects a programmed splicing switch associated with tumour development and relates to lack of differentiation rather than to a randomly selected trait.

While definitive proof of a driving role for any of these splicing events will require their *in vivo* manipulation in the natural context of a tumour, our data strongly suggest that overexpression of hnRNPH, possibly reflecting stem cell expression programs, is at the centre of an oncogenic splicing switch which modulates resistance to apoptosis and invasiveness—two hallmarks of malignant gliomas—and possibly other key aspects of aggressive tumour behaviour.

Materials and methods

Ethics statement

Collection and use of human tissues performed with consent from all participants, in accordance with IRB approved protocols of MSKCC.

Tissue sources

Human adult normal cerebral cortex RNA (donor information: N27, N0105, B130, N0109, N18) was purchased from BioChain. Normal tissue panel RNAs: whole brain, fetal brain, heart, kidney, liver, lung, placenta, prostate, salivary gland, skeletal muscle, thymus, thyroid, uterus and colon were from Clonetech (cat#636643).

Tumour samples

Tumours were snap-frozen in the operating room, and stored at −80°C. Samples in liquid nitrogen were ground and protein was extracted with M-per tissue extract solution (Pierce) with protease inhibitor cocktail tablets (Roche). Concentrations determined by BCA method (Bio-Rad).

Tissue culture

Human GBM T98G (ATCC, CRL-1690) and U373 cells (HTB-17), HeLa cells (CCL-2), IMR-90 (CCL-186), HUVEC (BD Biosciences) and HEK-293T (CRL-1573) were grown and maintained as recommended.

siRNA

Oligofectamine (Invitrogen) was used to transfect siRNAs as per the instructions, final concentration of siRNA was determined experimentally and did not exceed 200 μM. Control siRNA: siC #5 (Ambion).

siH and siH2 were used at a concentration of 50 μM each, siE16 at 100 μM. SiC was used at the total final concentration for the experiment. It was also added to other points so every treatment was at the same final concentration. Cells were treated for 24 h and then incubated for indicated times after media change. See Supplementary Table 1for sequences.

Transfections

Transfections were done with FUGENE 6 (Roche) as per the instructions.

Morpholino treatments

Morpholino oligomers (Gene Tools) were diluted in growth medium and added to cells. Endoporter (Gene Tools) was then added at 6 μM (final). HnRNPH (M4.3′/5′) and RON (M11.3′/5′) morpholinos were used at a concentration of 5 μM each (10 μM total). All treatments were performed with the same final concentration of morpholino using the morpholino control (MC) as filler. See Supplementary Table 1 for sequences.

RNA extraction

TRIZOL (Invitrogen) was used according to protocol. DNA was removed by TURBO DNA-free (Ambion). RNAqueous (Ambion) was used for recovery of RNA from small samples (from 24-well and smaller).

Polymerase chain reaction

In all, 1 μg of DNAse-treated total RNA (or 8 μl of RNA extracted with RNAqueous) was reverse transcribed with Superscript III RT using either Oligo d(T) (cell culture) or random hexamers (tissues). The cDNA was then used for PCR analysis. Platinum Taq Polymerase (Invitrogen) was used for detection of different splice variants. Conditions for PCRs were as per the instructions with an extension time of 1 min/1000 bp and an annealing temperature of 60°C. PCR products were separated on agarose gel, stained with ethidium bromide, photographed under UV light and quantified with NIH ImageJ. Primers (IDTDNA), used at a 0.2 μM, are reported in Supplementary Table 1.

Real-time qPCR

PCRs were performed as per the SYBR green (Invitrogen) instructions. Ribosomal Protein S3 (rps3) was used for normalization. The ddC(t) method was used for qPCR determination (Dussault and Pouliot, 2006). See Supplementary Table 1 for sequences.

Minigene construction

Human Genomic DNA (Promega) was amplified by Pfx (Invitrogen) for 35 cycles with an annealing temperature of 60°C and a 3′-extension time, using MADD-specific primers E15F and E17R, with *Eco*RI and *Not*I overhangs. RON minigene used E10F and E12R with the same overhangs. The resulting PCR products were gel purified, digested and subcloned into pcDNA3.1+ (Invitrogen). The ligation reaction was transformed into DH5α-competent cells. Plasmid DNA was prepared (Qiagen) and the resulting vectors were confirmed by restriction digests and sequencing.

Minigene mutants

Described mutants were made by site-specific mutagenesis by overlap extension (Molecular Cloning: A laboratory Manual, 3rd edn. Sambrook and Russell, pp 13.26–13.39). Detection of exogenously spliced MADD or RON was detected with an endogenous-specific forward primers and a plasmid-specific reverse primer (pINDr). See Supplementary Table 1 for sequences.

Westerns

Antibodies: hnRNPH N-16 (Santa Cruz, 1:1000), Caspase 8 559932 (BD Pharmingen, 1:3000), Actin AC-40 (Sigma, 1:1000), caspase 8 (BD Pharmingen, 559932, 1:3000), tubulin (Sigma, T5168, 1:10 000), hnRNP F 3H4 (GeneTex, 1:1000), SRSF1 AK103, Anti-HA (F7, Santa Cruz) bovine anti-goat HRP linked IgG (Santa Cruz Sc2378, 1:10 000), donkey anti-rabbit HRP linked IgG (GE healthcare NA934V, 1:10 000) and sheep anti-mouse HRP linked IgG (GE Healthcare NA931V, 1:10 000). Cells were extracted in M-per mammalian extraction reagent (Pierce) with Complete (Roche) protease inhibitors. Samples were normalized for protein amount by the Bradford assay (Bio-Rad) and subjected to SDS–PAGE. Proteins were transblotted by electrophoresis onto Immobilon-FL PVDF membrane (Millipore). Detection was done using SuperSignal West Femto Substrate (Thermo Scientific).

Electrophoretic mobility shift assays

EMSA was performed based on (Black DL *et al*. The electrophoretic mobility shift assay for RNA-binding proteins. In: RNA:Protein Interactions, A Practical Approach, pp 109–136). More details are available in the Supporting Information sections.

Invasion assay

Matrigel (BD biosciences) was used at 2 μg/8 μm pore size transwell insert (Falcon). Cells were treated as described above with morpholino oligos: Control (MC), hnRNPH (M4.3′ and M4.5′) or hnRNPH and RON (M11.3′ and M11.5′) for 72 h and then serum starved (DME 0% FBS) for 6 h. The cells were then trypsinized and counted and an equal number of live cells were plated per insert in 0% serum. Below the insert, DME with 10% FBS was plated as a chemoattractant. After 24 h, cells were fixed and stained with 20% methanol, 0.5% crystal violet. Photos of the complete inserts were taken, coded and all cells were counted blind with ImageJ. In all, 100 000 HeLa cells or 20 000 T98G cells were plated per insert, with three and five independent experiments performed in triplicates, respectively. Individual experiments were expressed as percent of average control and then average value from all treatments was calculated. *P*-value was determined by Student's *t*-test. Error bars are ± s.d.

Viability assay

HeLa cells were treated with siRNAs as described above; siC, siH/2 and siH/2 plus si16 were incubated for 24 h, media was changed and 48 h later (72 h from time of treatment) the cells were collected, coded and incubated with trypan blue (Cellgro) and at least four fields were counted blind for each independent treatment. Data were analysed by calculating the fold change in dead/total cells when compared with the control treatment and then the individual treatments were averaged for the final values. *P*-value was determined by Student's *t*-test. Error bars are ± s.d.

IHCs

Immunohistochemical staining was performed on 5 μm sections of formalin-fixed/paraffin-embedded tissues using an automated staining processor (Discovery XT, Ventana Medical Systems). HnRNPH antibody (Novus Biologicals, #NB100-2892) was diluted 1:300 in PBS 2% BSA. Images were acquired with a Nikon Eclipse E400 microscope connected to a Nikon Digital Slight camera system.

Supplementary data

Supplementary data are available at *The EMBO Journal* Online (http://www.embojournal.org).

Acknowledgements

We thank Mike Myers, Massimo Buvoli and Rotem Karni for comments and Hakim Djaballah of the MSKCC HTS Core Facility for siRNAs. This work was supported by funds from BTC and ETC at MSKCC. YXP supported by NIDA (DA013997 and DA029244), MS supported by a BTC grant.

Author contributions: CL, CB, EH and LC designed the experiments; CL, MS, SV, GR and YXP performed the experiments; CB and EH contributed reagents; CL and LC analysed data, CL and LC wrote the work.

Conflict of interest

The authors declare that they have no conflict of interest.

References

Al-Zoubi AM, Efimova EV, Kaithamana S, Martinez O, El-Idrissi Mel A, Dogan RE, Prabhakar BS (2001) Contrasting effects of IG20 and its splice isoforms, MADD and DENN-SV, on tumor necrosis factor alpha-induced apoptosis and activation of caspase-8 and -3. *J Biol Chem* **276:** 47202–47211

Boutz PL, Stoilov P, Li Q, Lin CH, Chawla G, Ostrow K, Shiue L, Ares Jr M, Black DL (2007) A post-transcriptional regulatory switch in polypyrimidine tract-binding proteins reprograms alternative splicing in developing neurons. *Genes Dev* **21:** 1636–1652

Bredel M, Bredel C, Juric D, Harsh GR, Vogel H, Recht LD, Sikic BI (2005) Functional network analysis reveals extended gliomagenesis pathway maps and three novel MYC-interacting genes in human gliomas. *Cancer Res* **65:** 8679–8689

Camacho-Vanegas O, Narla G, Teixeira MS, DiFeo A, Misra A, Singh G, Chan AM, Friedman SL, Feuerstein BG, Martignetti JA (2007) Functional inactivation of the KLF6 tumor suppressor gene by loss of heterozygosity and increased alternative splicing in glioblastoma. *Int J Cancer* **121:** 1390–1395

Caputi M, Zahler AM (2001) Determination of the RNA binding specificity of the heterogeneous nuclear ribonucleoprotein (hnRNP) H/H′/F/2H9 family. *J Biol Chem* **276:** 43850–43859

Cartegni L, Chew SL, Krainer AR (2002) Listening to silence and understanding nonsense: exonic mutations that affect splicing. *Nat Rev Genet* **3:** 285–298

Chen CD, Kobayashi R, Helfman DM (1999) Binding of hnRNP H to an exonic splicing silencer is involved in the regulation of alternative splicing of the rat beta-tropomyosin gene. *Genes Dev* **13:** 593–606

Cheung HC, Baggerly KA, Tsavachidis S, Bachinski LL, Neubauer VL, Nixon TJ, Aldape KD, Cote GJ, Krahe R (2008) Global analysis of aberrant pre-mRNA splicing in glioblastoma using exon expression arrays. *BMC Genomics* **9:** 216

Cheung HC, Corley LJ, Fuller GN, McCutcheon IE, Cote GJ (2006) Polypyrimidine tract binding protein and Notch1 are independently re-expressed in glioma. *Mod Pathol* **19:** 1034–1041

Cheung HC, Hai T, Zhu W, Baggerly KA, Tsavachidis S, Krahe R, Cote GJ (2009) Splicing factors PTBP1 and PTBP2 promote proliferation and migration of glioma cell lines. *Brain* **132:** 2277–2288

Chunduru S, Kawami H, Gullick R, Monacci WJ, Dougherty G, Cutler ML (2002) Identification of an alternatively spliced RNA for the Ras suppressor RSU-1 in human gliomas. *J Neurooncol* **60:** 201–211

Clower CV, Chatterjee D, Wang Z, Cantley LC, Vander Heiden MG, Krainer AR (2010) The alternative splicing repressors hnRNP A1/A2 and PTB influence pyruvate kinase isoform expression and cell metabolism. *Proc Natl Acad Sci USA* **107:** 1894–1899

Coutinho-Mansfield GC, Xue Y, Zhang Y, Fu XD (2007) PTB/nPTB switch: a post-transcriptional mechanism for programming neuronal differentiation. *Genes Dev* **21:** 1573–1577

Crooks GE, Hon G, Chandonia JM, Brenner SE (2004) WebLogo: a sequence logo generator. *Genome Res* **14:** 1188–1190

Dai C, Holland EC (2001) Glioma models. *Biochim Biophys Acta* **1551:** M19–M27

David CJ, Chen M, Assanah M, Canoll P, Manley JL (2010) HnRNP proteins controlled by c-Myc deregulate pyruvate kinase mRNA splicing in cancer. *Nature* **463:** 364–368

Dussault AA, Pouliot M (2006) Rapid and simple comparison of messenger RNA levels using real-time PCR. *Biol Proced Online* **8:** 1–10

Efimova EV, Al-Zoubi AM, Martinez O, Kaithamana S, Lu S, Arima T, Prabhakar BS (2004) IG20, in contrast to DENN-SV, (MADD splice variants) suppresses tumor cell survival, and enhances their susceptibility to apoptosis and cancer drugs. *Oncogene* **23:** 1076–1087

Faustino NA, Cooper TA (2003) Pre-mRNA splicing and human disease. *Genes Dev* **17:** 419–437

Fisette JF, Toutant J, Dugre-Brisson S, Desgroseillers L, Chabot B (2010) hnRNP A1 and hnRNP H can collaborate to modulate 5′ splice site selection. *RNA* **16:** 228–238

Fogel BL, McNally MT (2000) A cellular protein, hnRNP H, binds to the negative regulator of splicing element from Rous sarcoma virus. *J Biol Chem* **275:** 32371–32378

Ghigna C, Giordano S, Shen H, Benvenuto F, Castiglioni F, Comoglio PM, Green MR, Riva S, Biamonti G (2005) Cell motility is controlled by SF2/ASF through alternative splicing of the Ron protooncogene. *Mol Cell* **20:** 881–890

Ghigna C, Valacca C, Biamonti G (2008) Alternative splicing and tumor progression. *Curr Genomics* **9:** 556–570

Hambardzumyan D, Amankulor NM, Helmy KY, Becher OJ, Holland EC (2009) Modeling adult gliomas using RCAS/t-va technology. *Transl Oncol* **2:** 89–95

Hanahan D, Weinberg RA (2000) The hallmarks of cancer. *Cell* **100:** 57–70

Hu X, Holland EC (2005) Applications of mouse glioma models in preclinical trials. *Mutat Res* **576:** 54–65

Hua Y, Vickers TA, Okunola HL, Bennett CF, Krainer AR (2008) Antisense masking of an hnRNP A1/A2 intronic splicing silencer corrects SMN2 splicing in transgenic mice. *Am J Hum Genet* **82:** 834–848

Huang H, Held-Feindt J, Buhl R, Mehdorn HM, Mentlein R (2005) Expression of VEGF and its receptors in different brain tumors. *Neurol Res* **27:** 371–377

Jin W, Cote GJ (2004) Enhancer-dependent splicing of FGFR1 alpha-exon is repressed by RNA interference-mediated down-regulation of SRp55. *Cancer Res* **64:** 8901–8905

Kanu OO, Hughes B, Di C, Lin N, Fu J, Bigner DD, Yan H, Adamson C (2009) Glioblastoma multiforme oncogenomics and signaling pathways. *Clin Med Oncol* **3:** 39–52

Karni R, de Stanchina E, Lowe SW, Sinha R, Mu D, Krainer AR (2007) The gene encoding the splicing factor SF2/ASF is a proto-oncogene. *Nat Struct Mol Biol* **14:** 185–193

Kinali M, Arechavala-Gomeza V, Feng L, Cirak S, Hunt D, Adkin C, Guglieri M, Ashton E, Abbs S, Nihoyannopoulos P, Garralda ME, Rutherford M, McCulley C, Popplewell L, Graham IR, Dickson G, Wood MJ, Wells DJ, Wilton SD, Kole R *et al* (2009) Local restoration of dystrophin expression with the morpholino oligomer AVI-4658 in Duchenne muscular dystrophy: a single-blind, placebo-controlled, dose-escalation, proof-of-concept study. *Lancet Neurol* **8:** 918–928

Kong DS, Song SY, Kim DH, Joo KM, Yoo JS, Koh JS, Dong SM, Suh YL, Lee JI, Park K, Kim JH, Nam DH (2009) Prognostic significance of c-Met expression in glioblastomas. *Cancer* **115:** 140–148

Kurada BR, Li LC, Mulherkar N, Subramanian M, Prasad KV, Prabhakar BS (2009) MADD, a splice variant of IG20, is indispensable for MAPK activation and protection against apoptosis upon tumor necrosis factor-alpha treatment. *J Biol Chem* **284:** 13533–13541

Lee J, Kotliarova S, Kotliarov Y, Li A, Su Q, Donin NM, Pastorino S, Purow BW, Christopher N, Zhang W, Park JK, Fine HA (2006) Tumor stem cells derived from glioblastomas cultured in bFGF and EGF more closely mirror the phenotype and genotype of primary tumors than do serum-cultured cell lines. *Cancer Cell* **9:** 391–403

Liang Y, Diehn M, Watson N, Bollen AW, Aldape KD, Nicholas MK, Lamborn KR, Berger MS, Botstein D, Brown PO, Israel MA (2005) Gene expression profiling reveals molecularly and clinically distinct subtypes of glioblastoma multiforme. *Proc Natl Acad Sci USA* **102:** 5814–5819

Lim KM, Yeo WS, Chow VT (2004) Antisense abrogation of DENN expression induces apoptosis of leukemia cells *in vitro*, causes tumor regression *in vivo* and alters the transcription of genes involved in apoptosis and the cell cycle. *Int J Cancer* **109:** 24–37

Liu J, Beqaj S, Yang Y, Honore B, Schuger L (2001) Heterogeneous nuclear ribonucleoprotein-H plays a suppressive role in visceral myogenesis. *Mech Dev* **104:** 79–87

Lo HW, Zhu H, Cao X, Aldrich A, Ali-Osman F (2009) A novel splice variant of GLI1 that promotes glioblastoma cell migration and invasion. *Cancer Res* **69:** 6790–6798

Long JC, Caceres JF (2009) The SR protein family of splicing factors: master regulators of gene expression. *Biochem J* **417:** 15–27

Lu Y, Yao HP, Wang MH (2007) Multiple variants of the RON receptor tyrosine kinase: biochemical properties, tumorigenic activities, and potential drug targets. *Cancer Lett* **257:** 157–164

Manley JL, Krainer AR (2010) A rational nomenclature for serine/arginine-rich protein splicing factors (SR proteins). *Genes Dev* **24:** 1073–1074

Martinez-Contreras R, Cloutier P, Shkreta L, Fisette JF, Revil T, Chabot B (2007) hnRNP proteins and splicing control. *Adv Exp Med Biol* **623:** 123–147

Martinez-Contreras R, Fisette JF, Nasim FU, Madden R, Cordeau M, Chabot B (2006) Intronic binding sites for hnRNP A/B and hnRNP F/H proteins stimulate pre-mRNA splicing. *PLoS Biol* **4:** e21

Mauger DM, Lin C, Garcia-Blanco MA (2008) hnRNP H and hnRNP F complex with Fox2 to silence fibroblast growth factor receptor 2 exon IIIc. *Mol Cell Biol* **28:** 5403–5419

McLendon R, Friedman A, Bigner D, Van Meir EG, Brat DJ, Mastrogianakis GM, Olson JJ, Mikkelsen T, Lehman N, Aldape K, Yung WK, Bogler O, Weinstein JN, VandenBerg S, Berger M, Prados M, Muzny D, Morgan M, Scherer S, Sabo A *et al* (2008) Comprehensive genomic characterization defines human glioblastoma genes and core pathways. *Nature* **455:** 1061–1068

Mulherkar N, Prasad KV, Prabhakar BS (2007) MADD/DENN splice variant of the IG20 gene is a negative regulator of caspase-8 activation. Knockdown enhances TRAIL-induced apoptosis of cancer cells. *J Biol Chem* **282:** 11715–11721

Mulherkar N, Ramaswamy M, Mordi DC, Prabhakar BS (2006) MADD/DENN splice variant of the IG20 gene is necessary and sufficient for cancer cell survival. *Oncogene* **25:** 6252–6261

Ni JZ, Grate L, Donohue JP, Preston C, Nobida N, O'Brien G, Shiue L, Clark TA, Blume JE, Ares Jr M. (2007) Ultraconserved elements are associated with homeostatic control of splicing regulators by alternative splicing and nonsense-mediated decay. *Genes Dev* **21:** 708–718

Okunola HL, Krainer AR (2009) Cooperative-binding and splicing-repressive properties of hnRNP A1. *Mol Cell Biol* **29:** 5620–5631

Pan Q, Shai O, Lee LJ, Frey BJ, Blencowe BJ (2008) Deep surveying of alternative splicing complexity in the human transcriptome by high-throughput sequencing. *Nat Genet* **40:** 1413–1415

Prabhakar BS, Mulherkar N, Prasad KV (2008) Role of IG20 splice variants in TRAIL resistance. *Clin Cancer Res* **14:** 347–351

Salomonis N, Nelson B, Vranizan K, Pico AR, Hanspers K, Kuchinsky A, Ta L, Mercola M, Conklin BR (2009) Alternative splicing in the differentiation of human embryonic stem cells into cardiac precursors. *PLoS Comput Biol* **5:** e1000553

Shai R, Shi T, Kremen TJ, Horvath S, Liau LM, Cloughesy TF, Mischel PS, Nelson SF (2003) Gene expression profiling identifies molecular subtypes of gliomas. *Oncogene* **22:** 4918–4923

Shih AH, Dai C, Hu X, Rosenblum MK, Koutcher JA, Holland EC (2004) Dose-dependent effects of platelet-derived growth factor-B on glial tumorigenesis. *Cancer Res* **64:** 4783–4789

Sun L, Hui AM, Su Q, Vortmeyer A, Kotliarov Y, Pastorino S, Passaniti A, Menon J, Walling J, Bailey R, Rosenblum M, Mikkelsen T, Fine HA (2006) Neuronal and glioma-derived stem cell factor induces angiogenesis within the brain. *Cancer Cell* **9:** 287–300

Venables JP, Klinck R, Koh C, Gervais-Bird J, Bramard A, Inkel L, Durand M, Couture S, Froehlich U, Lapointe E, Lucier JF, Thibault P, Rancourt C, Tremblay K, Prinos P, Chabot B, Elela SA (2009) Cancer-associated regulation of alternative splicing. *Nat Struct Mol Biol* **16:** 670–676

Wagh PK, Peace BE, Waltz SE (2008) Met-related receptor tyrosine kinase Ron in tumor growth and metastasis. *Adv Cancer Res* **100:** 1–33

Wang E, Cambi F (2009) Heterogeneous nuclear ribonucleoproteins H and F regulate the proteolipid protein/DM20 ratio by recruiting U1 small nuclear ribonucleoprotein through a complex array of G runs. *J Biol Chem* **284:** 11194–11204

Wang E, Dimova N, Cambi F (2007) PLP/DM20 ratio is regulated by hnRNPH and F and a novel G-rich enhancer in oligodendrocytes. *Nucleic Acids Res* **35:** 4164–4178

Wu B, Li Y, Morcos PA, Doran TJ, Lu P, Lu QL (2009) Octaguanidine morpholino restores dystrophin expression in cardiac and skeletal muscles and ameliorates pathology in dystrophic mdx mice. *Mol Ther* **17:** 864–871

Yamada Y, Kuroiwa T, Nakagawa T, Kajimoto Y, Dohi T, Azuma H, Tsuji M, Kami K, Miyatake S (2003) Transcriptional expression of survivin and its splice variants in brain tumors in humans. *J Neurosurg* **99:** 738–745

Yamaguchi F, Saya H, Bruner JM, Morrison RS (1994) Differential expression of two fibroblast growth factor-receptor genes is associated with malignant progression in human astrocytomas. *Proc Natl Acad Sci USA* **91:** 484–488

Yeo GW, Xu X, Liang TY, Muotri AR, Carson CT, Coufal NG, Gage FH (2007) Alternative splicing events identified in human embryonic stem cells and neural progenitors. *PLoS Comput Biol* **3:** 1951–1967

Yu Y, Jiang X, Schoch BS, Carroll RS, Black PM, Johnson MD (2007) Aberrant splicing of cyclin-dependent kinase-associated protein phosphatase KAP increases proliferation and migration in glioblastoma. *Cancer Res* **67:** 130–138